Hindawi
Journal of Nanomaterials
Volume 2022, Article ID 2990466, 13 pages
https://doi.org/10.1155/2022/2990466

Research Article

Study of the Potential of La/Bi_2S_3 Catalyst for Photodegradation of Acid Yellow 42 Dye under Visible Light

Ernso Fenelon,[1] **Achmad Chusnun Ni'am**,[2] **Ya-Fen Wang**,[3,4] **and Sheng-Jie You**[3,4]

[1]*Centre de Recherche Interdisciplinaire Pour la Vulgarisation Agricole et le Développement Local (CREIVADEL), Université Notre Dame d'Haïti, Faculté d'Agronomie, BP HT 8110, Redon, Torbeck, Haiti*
[2]*Department of Environmental Engineering, Institut Teknologi Adhi Tama Surabaya, Arief Rachman Hakim Road No. 100, Surabaya 60117, Indonesia*
[3]*Department of Environmental Engineering, Chung Yuan Christian University, Chung Li, 320 Taoyuan, Taiwan*
[4]*Center for Environmental Risk Management, Chung Yuan Christian University, 200 Chung Pei Road, Chungli 320, Taiwan*

Correspondence should be addressed to Ernso Fenelon; efenelon62@gmail.com and Sheng-Jie You; sjyou@cycu.edu.tw

Received 15 July 2022; Revised 16 September 2022; Accepted 22 September 2022; Published 6 October 2022

Academic Editor: Osman Ahmed Zelekew

The new catalyst (La/Bi_2S_3) applies for the photodegradation of Acid Yellow 42 (AY42) dye under visible light in this study. The La/Bi_2S_3 material is the motivating catalyst due to the excellent ability of Lanthanum (La) to increase the adsorption capacity and electron-hole separation of Bi_2S_3 for enhancing the degradation of AY42. The characterization analysis of the prepared material confirms a successful synthesis using the hydrothermal method. The efficiency of photodegradation AY42 using La/Bi_2S_3 is higher than pure Bi_2S_3. La on Bi_2S_3 (doped at 3%), which is devised on adsorption (40.24%) and photodegradation (51.86%), has the best degradation efficiency (92.1%). The trapping experiment and the analysis of electron spin resonance (ESR) spectra explain that the hydroxyl radical is the most active species in this photocatalytic process due to the total degradation efficiency decreasing from 92.1% to 57.16% by the scavenger using isopropyl alcohol (IPA). The hole (h^+) shows its importance in the photodegradation of AY42 by detecting that OH^- is the intermediate species. The new material (La/Bi_2S_3) also shows excellent photostability in the reusability test. Finally, the result confirms that La is a suitable doping metal for Bi_2S_3 and is interesting for practical application under visible light. The new catalyst (La/Bi_2S_3) applies for the photodegradation of Acid Yellow 42 (AY42) dye under visible light in this study. The La/Bi2S3 material is the motivating catalyst due to the excellent ability of Lanthanum (La) to increase the adsorption capacity and electron-hole separation of Bi_2S_3 for enhancing the degradation of AY42. The characterization analysis of the prepared material confirms a successful synthesis using the hydrothermal method. The photodegradation efficiency of AY42 using La/$Bi_2S_3$is higher than pure Bi_2S_3. The doping of 3% weight of La on Bi_2S_3 shows the optimum degradation efficiency of 92.1%, devised on adsorption (40.24%) and photodegradation (51.86%). The pure Bi_2S_3 (46.7%) contains 17.1% of adsorption and 29.6% of photodegradation. The trapping experiment and the analysis of electron spin resonance (ESR) spectra explain that the hydroxyl radical is the most active species in this photocatalytic process due to the total degradation efficiency decreasing from 92.1% to 57.16% by the scavenger using isopropyl alcohol (IPA). The hole (h^+) shows its importance in the photodegradation of AY42 by detecting that OH^- is the intermediate species. The new material (La/Bi_2S_3) also shows excellent photostability in the reusability test. Finally, the result confirms that La is a suitable doping metal for Bi_2S_3 and is interesting for practical application under visible light.

1. Introduction

Dye degradation is among the most complicated tasks for textile processing plants. Hundreds of synthetic colors are employed in the industry, some carcinogenic [1]. Among these dyes, azo dyes are considered the most persistent and dangerous industrial pollutants due to their ability to contaminate natural water [2]. It is the most utilized dyes, accounting for more than 60% of all commercially available dyes [3, 4]. Among the azo dyes, Acid Yellow 42 (AY42) is a commercial dye mainly used for wool dyeing, silk, glue printing, polyamide fiber dyeing, leather shading, inks for printing, food colorants, hair dye, tattoo inks, cosmetics, textiles, and colors for drugs [5]. So far, only a few preliminary

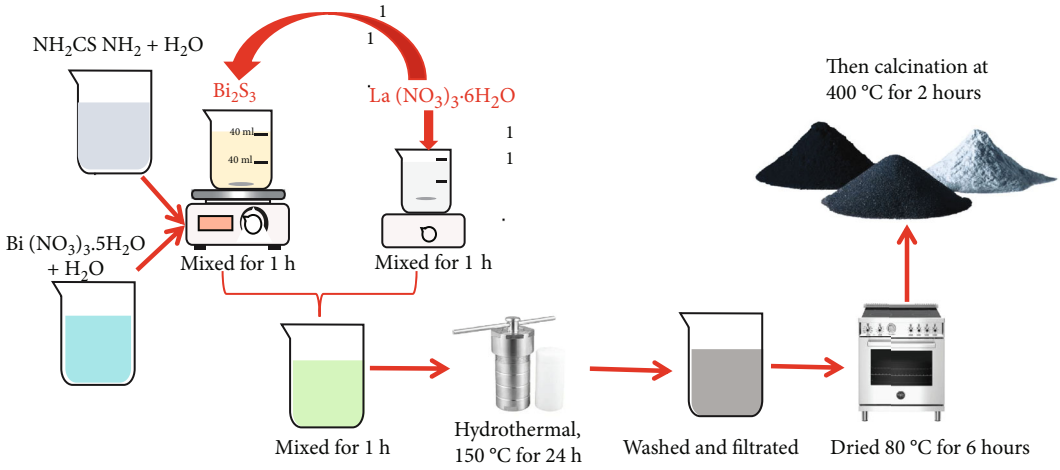

Figure 1: Synthesis of La/Bi_2S_3 composites.

studies have been conducted about a treatment method for the degradation of this target pollutant (AY42). The mineralization degradation of AY42 demonstrated a high degradation by adsorption [6]. However, the calcination method is not environmentally friendly as it produces air pollution and consumes a lot of energy [7]. It uses turnip peroxidases and enzymes that require the 1-hydroxy benzotriazole (HOBT) to decolorize most of the acid dyes [8].

Importantly, photocatalysis exhibits a successful way of treating industrial effluent [9]. The photocatalyst is rapidly expanding and is significantly efficacious due to the number of benefits, including environmental protection and total elimination of pollution [10]. The photocatalytic process promotes the oxidation and removal of most organic compounds, potentially allowing the complete elimination of organic contaminants [11]. The types of semiconductor catalysts, such as TiO_2, WO_3, ZnO, SnO_2, CeO_2, Bi_2S_3, and $BiVO_4$ photocatalysts, are commonly used [12] but are limited by large bandgaps or fast recombination of electron-hole pairs. Recently, more attention has been received from visible light photocatalysts, specifically materials containing bismuth [13]. Bismuth-based photocatalysts are commonly studied as visible photocatalysts guided by light, such as Bi_2O_3, $BiVO_4$, Bi_2WO_6, Bi_2S_3, and Bi-$ZnWO_4$ [14, 15]. Amid the catalysts, Bi_2S_3 is among the most efficient semiconductors and draws broad attention to Schottky diode [16], solar cells [17], sensors [18], supercapacitor electrodes [19], and thermoelectric devices [20]. Bi_2S_3 has a narrow bandgap of 1.3 eV and an excellent absorption coefficient for photocatalytic activities under visible light [21]. The photocatalytic of Bi_2S_3 is restricted due to the quick recombination of photoinduced electron-hole pairs [22].

According to the above limitation, the new dopant material (Lanthanum) is used to improve the ability of Bi_2S_3 in photocatalytic activities in this study. Due to the excellent command of lanthanum (La), which enhances the capacity of the material, some preview studies mentioned that La has a synergistic effect and influence to capture photoinduced electrons [23, 24] that are used to enhance the redox, textural, and structural aspects of the material [25]. In addition, La enhances the catalyst's ability and modifies the material's structure to demonstrate a high light absorption spectrum and to increase the electron-hole separation ability [23, 26, 27]. In the present study, La/Bi_2S_3 composite was prepared by hydrothermal method, and the performance of La/Bi_2S_3 was evaluated by different kinds of experiments, such as photocatalytic degradation activities of AY42, the effect of dyes concentration, catalyst amount, recycle test, and trapping test. La inhibits the recombination of photogenerated electron-hole pairs of Bi_2S_3 and improves the photodegradation performance of the prepared material. Thus, the La/Bi_2S_3 composite shows a great perspective and contribution to increasing photocatalytic activity under visible light.

2. Experimental Section

2.1. Reagents and Materials. This experiment used various chemicals: Bismuth nitrate (Bi $(NO_3)_3{\cdot}5H_2O$) (mass fraction 0.990) was extended in China, thiourea (CH4N2S, China, 99.9%), isopropyl alcohol (IPA, Merck, 99.99%), potassium iodide (PubChem CID: 4875), and Acid Yellow 42 (PubChem CID: 228665). Table S1 details the structure of AY42 dye and demonstrates its degradation ability by the photocatalytic process due to its high carbon content. The ultra-pure water system of PURELAB flex 3 is used as the source for deionized water.

2.2. Preparation of Bi_2S_3 and La/Bi_2S_3. The synthesis of Bi_2S_3 has followed the previous study [28]: 3.881 g of $Bi(NO_3)_3.5H_2O$ diluted in 100 mL of double-distilled water (DDW) and 20 mL of DDW mixed with 0.90 g of thiourea for 20 min separately; then, the solution of thiourea was dropped into the solution of $Bi(NO_3)_3.5H_2O$ and then mixed at 60 °C for 30 min. Finally, the yellow solution was mixed at room temperature for 60 min and inserted in an autoclave at 150 °C for 24 hours. Afterward, the solid was recovered, filtered, and washed four times using DDW and ethanol ratio 5 : 1 to remove all the impurities. The final Bi_2S_3 dried at 60 °C for 10 hours. Furthermore, Bi_2S_3 calcinated for 2 hours at 400 °C to evaporate all the water in the material's pores.

La/Bi_2S_3 was synthesized by adding a different percentage of La weight % (1, 3, 5, and 7) using $La(NO_3)_3.6H_2O$ as a

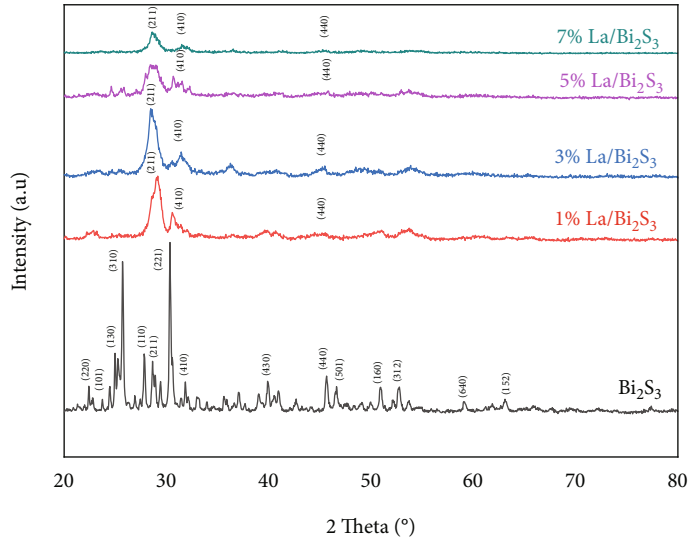

Figure 2: The XRD analysis of as-prepared materials.

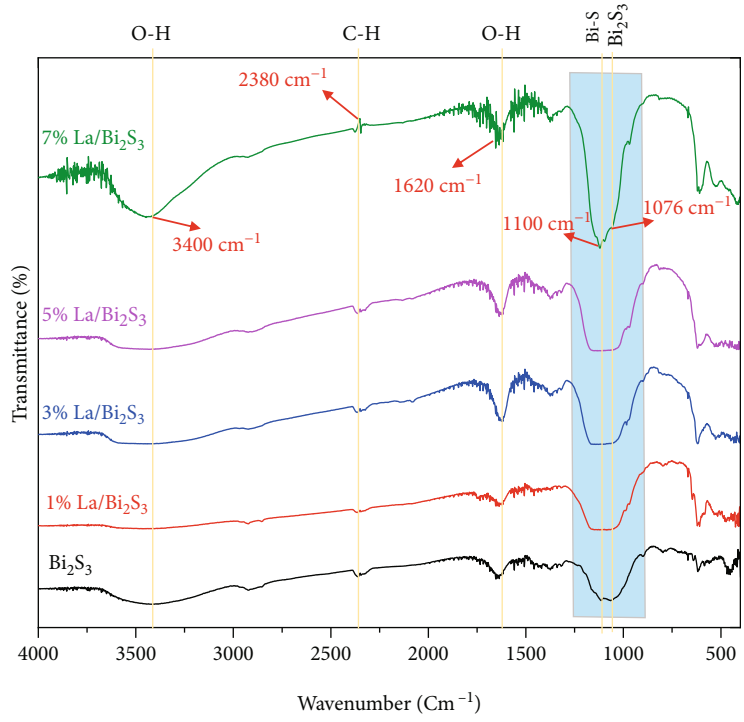

Figure 3: FTIR analysis of Bi_2S_3 and La/Bi_2S_3.

precursor into the mixture solution of Bi_2S_3. After achieving room temperature, it was stirred for 60 min and finally mimicked the exact condition of the hydrothermal, washing, drying, and calcination process to acquire La/Bi_2S_3. Figure 1 shows the synthesis procedure to synthesize the La/Bi_2S_3.

2.3. Characterization Techniques. Scanning electron microscopy (SEM) was used to observe the surface morphology of the material. The X-ray diffraction (XRD) pattern was studied to analyze the phase composition and crystalline structure. FT/IR-4700 FTIR Spectrometer from JASCO was used to determine the function group and the bonding materials. The instrument JEM 1400 JEOL was used to measure transmission electron microscopy (TEM) and observe the catalyst's morphology. The electron spin resonance (ESR) was analyzed using a 5,5-dimethyl-1-pyrroline-N-oxide (DMPO) agent.

2.4. Photocatalytic Degradation Activities. The research on photodegradation of AY42 under visible light using La/Bi_2S_3 was studied at the different weight percentages of La/doped on Bi_2S_3 (1% La/Bi_2S_3, 3% La/Bi_2S_3, 5% La/Bi_2S_3, and 7% La/Bi_2S_3) and was tested using 0.02 g of catalysts in

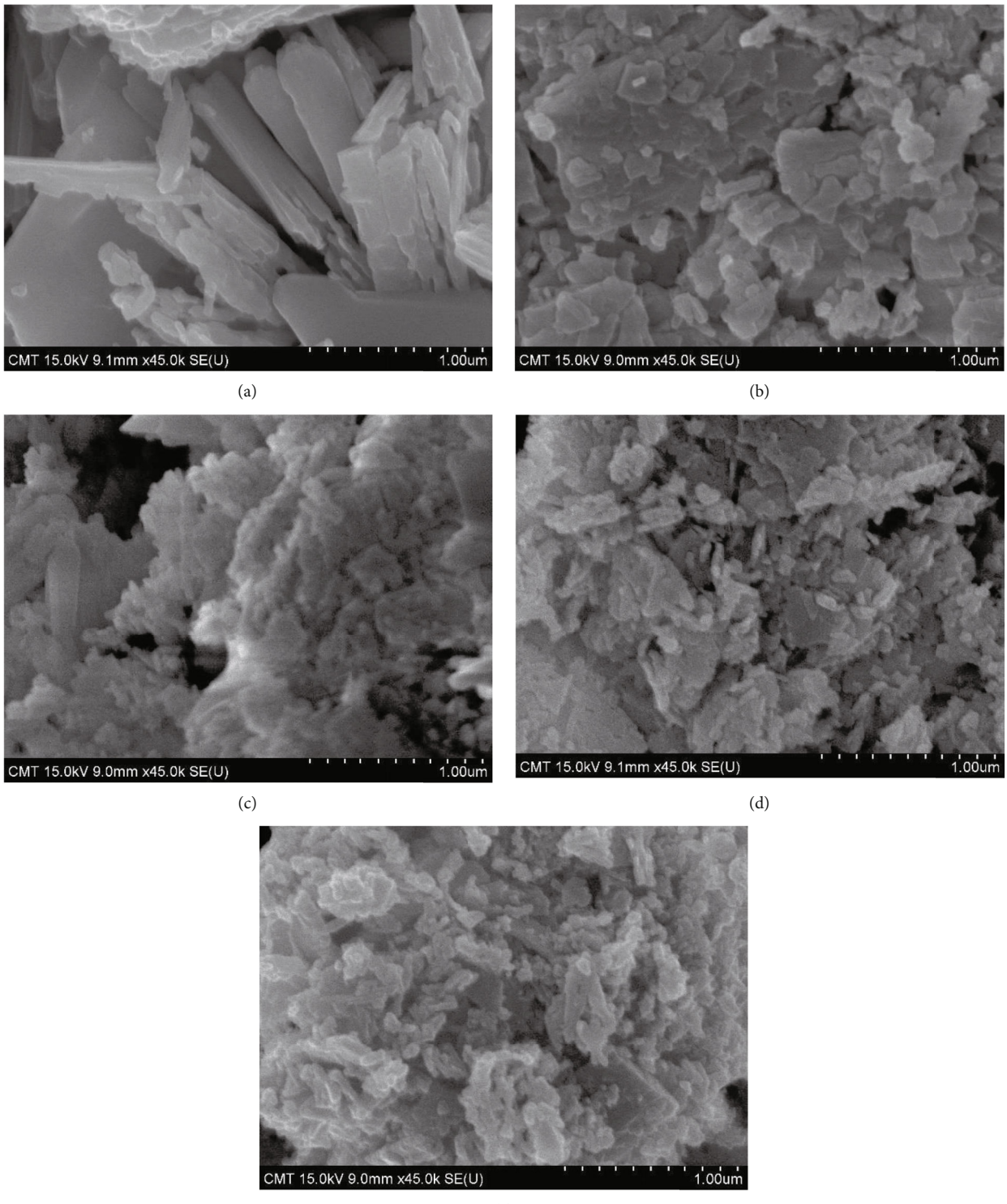

Figure 4: SEM images analysis of Bi_2S_3 (a), 1% La/Bi_2S_3 (b), 3% La/Bi_2S_3 (c), 5% La/Bi_2S_3 (d), and 7% La/Bi_2S_3 (e).

all experiments. For all experiments, a beaker glass was applied as a reactor, and 60 mL of AY42 solution was introduced at initial concentrations of 10 mg L^{-1}. The liquid solution was placed in the dark for 30 min for adsorption and desorption of the catalyst. Finally, the photocatalytic activity was irradiated under visible light for 75 min, and the dye was analyzed at the interval of 15 min. A light emitting diode (LED) lamp of 42 volts with 7000 lm, and the wavelength (λ) ≥420 nm was applied for the visible light source, and a UV-vis spectrometer measured AY42 removal at 410 nm wavelengths. All the photocatalytic measurements were performed at room temperature and repeated twice to calculate

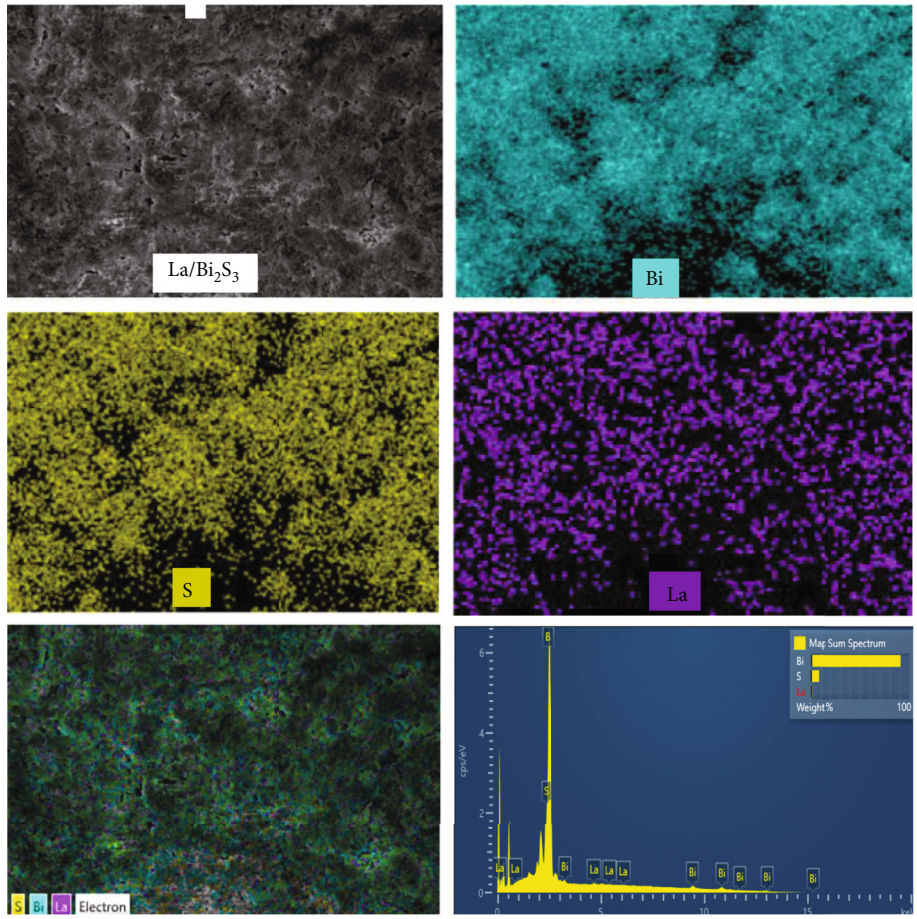

Figure 5: Analysis of energy-dispersive spectroscopy (EDS) of La/Bi_2S_3 composites.

the error bars in the result of the experiment. The photocatalytic degradation of AY42 (η) is obtained by $C/C0$, where $C0$ is the initial optimum absorbance (λ) of AY42 ($\lambda = 410\,nm$) of the UV-vis and C is the outlet absorbance at any time. A trapping test was realized by adding different scavengers of 10^{-3} M into the solution of AY42 content 0.02 g of the catalyst. Potassium dichromate ($K_2Cr_2O_7$), isopropyl alcohol (IPA), and potassium iodide (KI) were applied as effective scavengers to control the photogenerated electron, hydroxyl radical, and the hole, respectively. The recycle test was realized by reusing four times the same material by selecting the best sample to analyze the stability of the as-prepared material. The kinetics first-order was studied using $\ln(C/C0) = kt$ to measure the degradation rate of the pollutant and calculated using the absorbance of AY42 at the initial C0 after getting the adsorption and desorption in the dark and also the final concentration of AY42 at time t (min).

The degradation capacities of AY42 under visible light over La/Bi_2S_3 material are observed by calculating in the following equation:

$$qe = \frac{(C0 - Ce) \times V}{m}. \quad (1)$$

qe ($mg\,g^{-1}$) is the degradation capacity of the catalyst. $C0$ and Ce ($mg\,L^{-1}$) are the initial and equilibrium concentrations of the AY42, respectively. V (L) is the volume of the AY42, and m (g) is the weight of the catalyst.

3. Results and Discussion

3.1. Analysis of XRD Pattern. The analysis of the XRD pattern of the Bi_2S_3 and La/Bi_2S_3 composites presented in Figure 2 exhibits the crystalline structure. The pure Bi_2S_3 showed various peaks at 22.41°, 23.69°, 24.9°, 25.8°, 28.65°, 30.39°, 31.86°, 39.88°, 45.7°, 46.67°, 50.98°, 52.82°, 59.10°, and 63.09° which can be related to the diffraction peaks at (220), (101) (130), (310), (211), (221), (410), (430), (440), (501), (160), (312), (640), and (152) planes of phase, indicating the orthorhombic Bi_2S_3 (JCPDS No. 170320) crystalline structure. The XRD analysis proved that the presence of La in Bi_2S_3 decreased the crystallite size of the catalyst. For further studies, the particle size was analyzed to confirm that the reduction of the crystallite size developed when La-doped the material. However, adding La increased the intensity of the (211) plane of Bi_2S_3 at the diffraction peak $2 = 28.65\circ$. It indicated the bias of orientations of these crystallographic planes [29]. The 211 facets were the most dominant in Bi_2S_3, suggesting the formation of microsphere

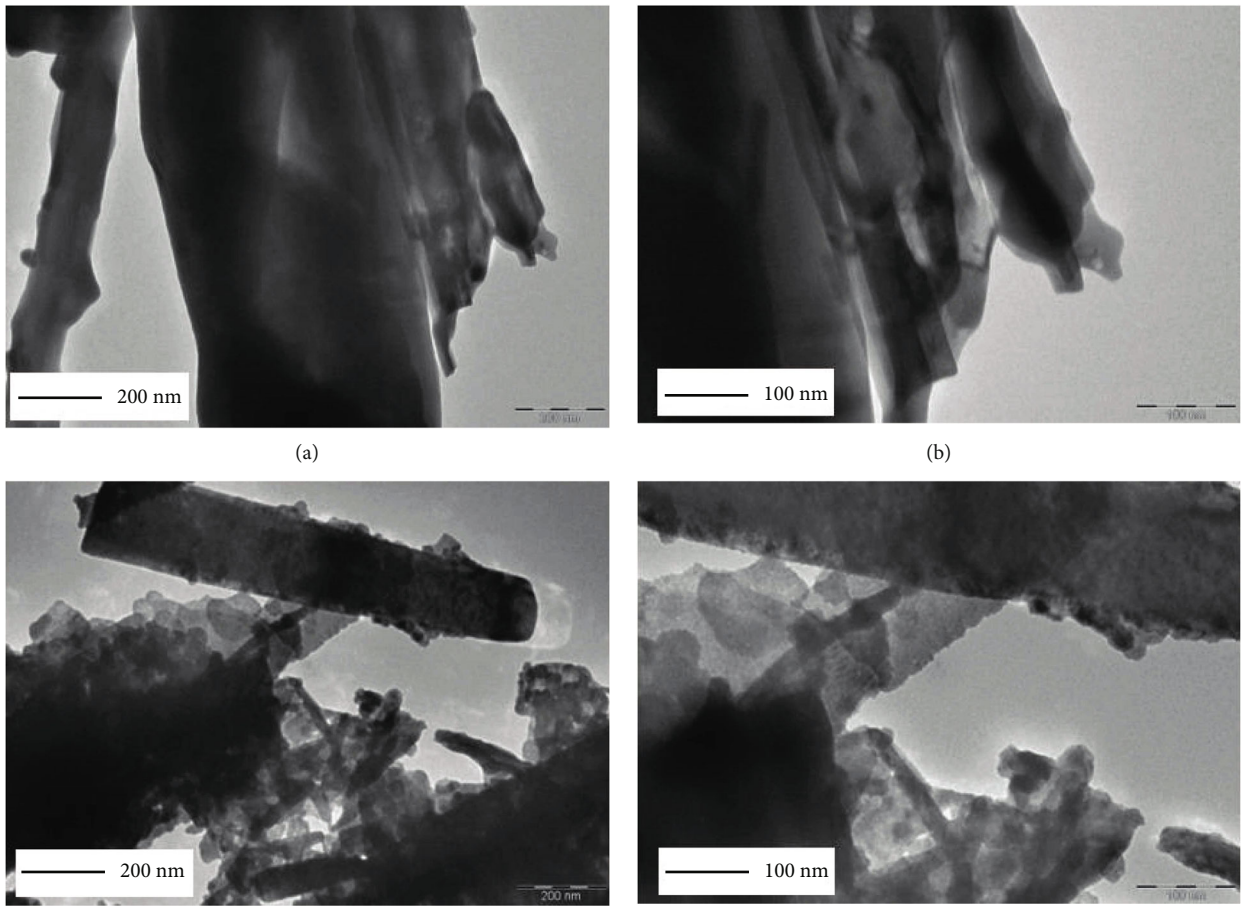

(a) (b) (c) (d)

Figure 6: Image analysis TEM of Bi_2S_3 (a, b) and 3% La/Bi_2S_3 (c, d).

particles [30]. This result shows that the excess amount of La could harm the photocatalytic activities of La/Bi_2S_3.

3.2. FTIR Analysis of Bi_2S_3 and La/Bi_2S_3. Figure 3 shows the FTIR analysis of Bi_2S_3 and La/Bi_2S_3. The vibration bands around 1076 cm^{-1} and 1100 cm^{-1} showed evidence of the apparition of Bi_2S_3 [28, 31] and ascribed to Bi-S bonds [21], respectively. The band around 1620 cm^{-1} is related to the (O-H) bending vibrations of the molecularly adsorbed water [32]. The peak of about 2380 cm^{-1} is responsible for the stretching vibrations of C–H [33]. The wavelength at 3400 cm^{-1} due to the O-H vibration is related to the water inside the samples [21]. The bands at 1076-1100 cm^{-1} became stronger as the amount of lanthanum in the composite increased. The modification of the bands' vibration of the Bi_2S_3 might explain the presence of La in the composite, and the XRD analysis could also confirm it.

3.3. Morphology of Bi_2S_3 and La/Bi_2S_3 Composites. Figure 4 shows the results of the SEM image of Bi_2S_3 and the different composites of La/Bi_2S_3. The pure microspheres Bi_2S_3 (Figure 4(a)) showed a particle size reduction while increasing the amount of La in the composite. Due to the material's particle size reduction, an excessive amount of La can be depicted on the surface of Bi_2S_3 in the images of 5% and 7% percent La/Bi_2S_3, respectively. The high percentage of La in the composite could present a negative effect by reducing the active species and providing the recombination electron hole of pure Bi_2S_3 photocatalyst.

Material processing and degradation reports of AY42 show that the particle size distribution of Bi_2S_3 and La/Bi_2S_3 grades was an essential metric. The particle sizes of Bi_2S_3 and La/Bi_2S_3 materials were analyzed using a Nano Zetasizer ZS by Malvern Panalytical. The average size of Bi_2S_3, 1% La/Bi_2S_3, 3% La/Bi_2S_3, 5% La/Bi_2S_3, and 7% La/Bi_2S_3 were 4.88, 3.22, 2.05, 1.08, and 1.63 μm, respectively. The particle size result confirms that the XRD pattern of Bi_2S_3 changes significantly with the presence of La due to the significant decrease of the particle size of pure Bi_2S_3 with the presence of La. The SEM images present that the addition of La-doped of Bi_2S_3 decreased the crystallites of the compound and might increase the active site of the material for better photocatalytic activities in the degradation of AY42 under visible light.

The elemental mapping analysis shown in Figure 5 was measured to support the SEM images to confirm the presence of all elements in as-prepared material. The blue color was represented by bismuth (Bi), yellow was the sulfur (S), and purple by the presence of La in the composites. The mixed colors indicated that all the elements (Bi, S, and La)

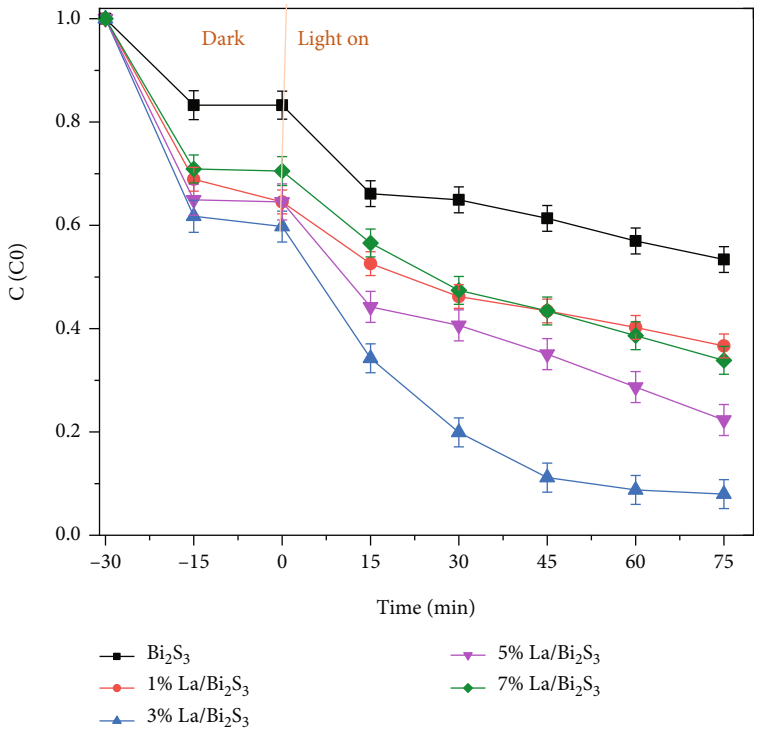

(a)

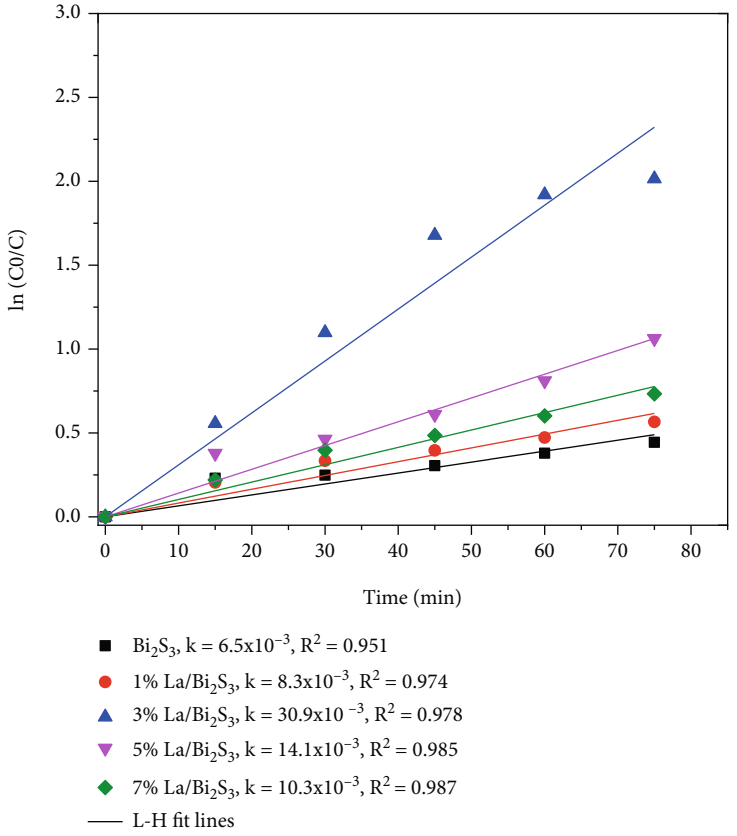

(b)

Figure 7: Continued.

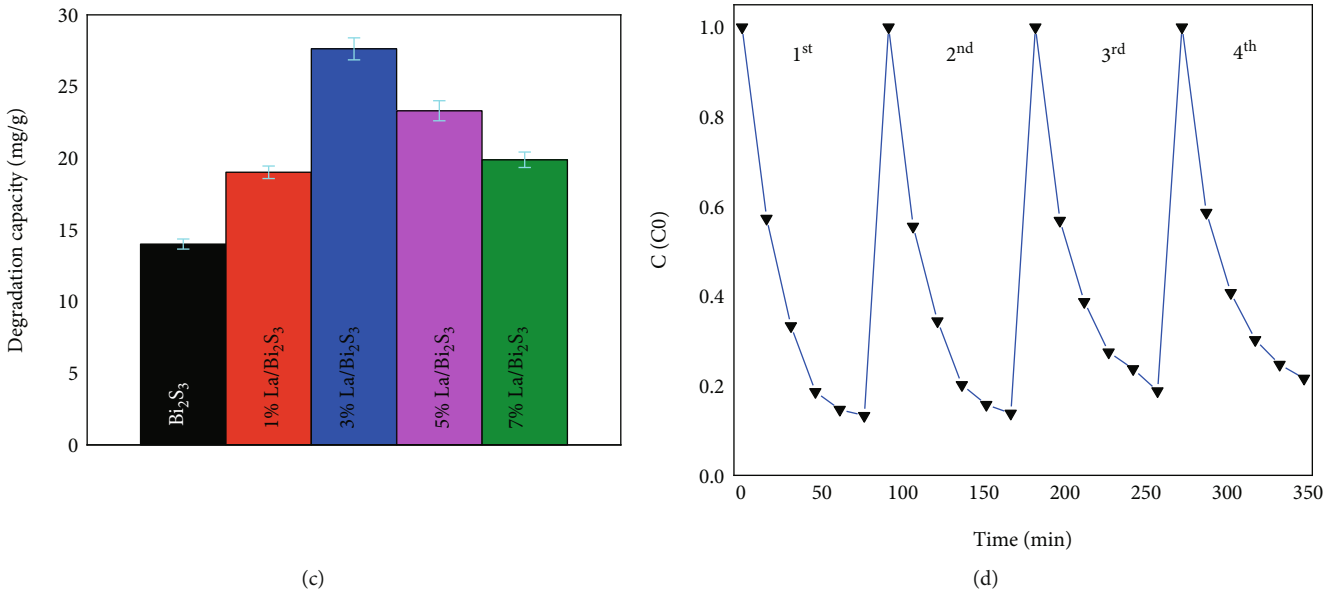

Figure 7: (a) Photodegradation activity of AY42 by Bi_2S_3 and La/Bi_2S_3 composites, (b) the degradation rate under visible light, (c) degradation capacity, and (d) reusability test for photocatalytic degradation of AY42 over 3% La/Bi_2S_3.

were present in the map of the SEM image, which confirmed the synthesis of La/Bi_2S_3 composite by the hydrothermal method. In the analysis result of the composite, the impurity detected was lower. So the composite morphology confirmed the successful synthesis of La/Bi_2S_3 material for photocatalytic activity.

The TEM analysis was studied by pure Bi_2S_3 and 3% La/Bi_2S_3. TEM analysis for 3% La/Bi_2S_3 shows evidence that La modified the morphology of Bi_2S_3 and the smaller particle size is formed for the benefits of the photocatalytic performance of the material. As a result, La worked to reduce the particle size of pure Bi_2S_3. The morphology of the prepared samples of pure Bi_2S_3 (Figures 6(a) and 6(b)) appearing in one block finally changed by adding La to the material, as shown in Figures 6(c) and 6(d) to improve the surface of distribution for more sites of active species to achieve a better photocatalytic activity of the material, so the TEM images proved the presence of La in the Bi_2S_3 material.

3.4. Photodegradation of Acid Yellow 42 under Visible Light by La/Bi_2S_3. The photodegradation experiment in Figure 7(a) reports a different percentage weight of La-doped on Bi_2S_3. The degradation of the pollutant was performed in the dark and the light for a better understanding of the catalyst. The result also shows that the catalyst also adsorbs a part of the AY42 due to the pores on the surface of the catalyst afterward, the photodegradation in the presence of the visible light. The total performance of pure Bi_2S_3, 1% La/Bi_2S_3, 3% La/Bi_2S_3, 5% La/Bi_2S_3, and 7% La/Bi_2S_3 resulted into 46.7%, 63.4%, 92.1%, 77.7%, and 66.3%, respectively. In this study, we found that the photodegradation increased when the amount of La-doped on Bi_2S_3 was increased from 1% to 3%. The decreasing efficiency of AY42 was detected by increasing the percentage of La (>3%) doped on Bi_2S_3. Since the absorbing and scattering catalyst photon increased by an excess of La in the photocatalytic process [27], the degradation rates were calculated by applying the kinetic first order (Figure 7(b)). The kinetic study shows that the degradation rate of the outstanding samples (3% La/Bi_2S_3) was better than the pure Bi_2S_3. It is explained that the presence of La also enhanced the removal rate under visible light. The degradation capacity was calculated to evaluate the mass in milligram (mg) of AY42 dyes that a specific weight can degrade in gram (g) of La/Bi_2S_3 catalyst under visible light. The calculation analysis is shown in Figure 7(c) that the degradation capacity of Bi_2S_3, 1% La/Bi_2S_3, 3% La/Bi_2S_3, 5% La/Bi_2S_3, and 7% La/Bi_2S_3 was 14.01 mg g^{-1}, 19.02 mg g^{-1}, 27.63 mg g^{-1}, 23.31 mg g^{-1}, and 19.89 mg g^{-1}, respectively; the percentage of error bars of the photocatalytic degradation of AY42 was around ±2.3% to ±3%. The degradation capacity of AY42 over La/Bi_2S_3 was compared with some previous studies in Table 1.

The recycle test was studied to analyze the photocatalytic stability of La/Bi_2S_3. La/Bi_2S_3 3% was selected as the focus sample; as we can denote in Figure 7(d), there is no difference from the first to the third that was recycled, and it slightly decreased with the difference value of 7% between the first and the fourth. This decrease results from the remaining pollutant on the catalyst's surface during the adsorption process. Therefore, the material La/Bi_2S_3 proved to show reasonable stability over the degradation of AY42. Besides the performance of La/Bi_2S_3 catalyst, it was also very competitive compared to some previous studies in Table 1 using Bi_2S_3 as base catalyst under visible-light-induced photodegradation of organic pollutant in the wastewater, and mostly better than the previous studies. It is concluded that La is an excellent doping metal for Bi_2S_3 in photocatalytic activities and shows the first application of the photocatalyst in degrading AY42 dye under visible light.

Table 1: Comparison of photodegradation of dyes based on Bi_2S_3 and Lanthanum under visible light.

Catalyst	Pollutants	Concentration (ppm)	Catalyst amount (mg)	Volume (ml)	Removal (%)	Mg/g	Time (min)	Mg/g/min	References
Bi_2S_3/Bi_2WO_6	Phenol	20	0.05	50	51.6	10.32	120	0.086	[37]
Cu/Bi_2S_3	Methylene blue	20	0.01	30	90.7	54.42	200	0.272	[38]
$BiPO_4/Bi_2S_3$	Methylene blue	10	0.05	100	80	16	180	0.089	[39]
$Bi_2S_3/Bi_2O_3/BOC$	Methyl orange	20	0.05	100	99	39.6	60	0.66	[40]
$SnO_2/Bi_2S_3/BiOCl–Bi_{24}O_{31}Cl_{10}$	Rhodamine B	10	0.02	60	80.8	24.24	180	0.135	[28]
Bi_2S_3/Bi_2Sn_2O7	Rhodamine B	5	0.05	50	94.4	4.72	360	0.013	[41]
La/Bi_2S_3	Acid yellow 42	10	0.02	60	92.1	27.63	75	0.368	This study

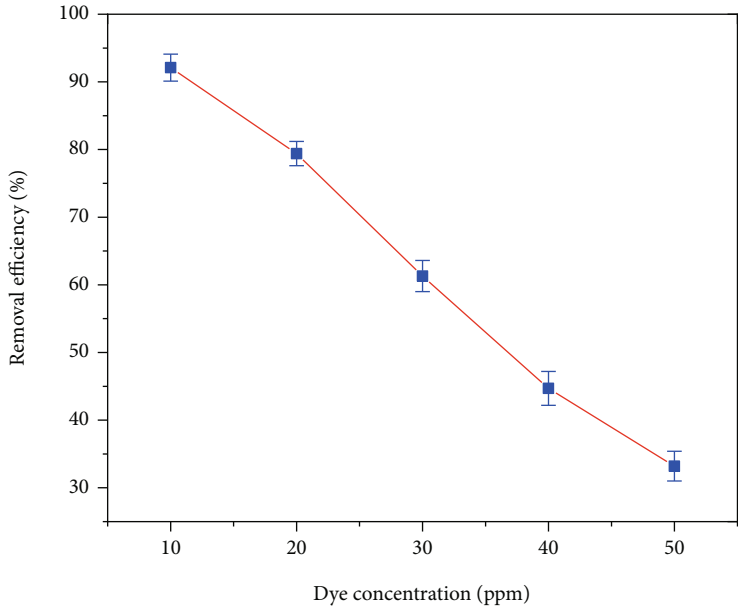

Figure 8: Effect of AY42 dyes concentration.

3.5. Effect of AY42 Dye Concentration. Figure 8 shows the result of the experiment of the effect of AY42 dye concentration realized with 20 mg of 3% La/Bi_2S_3 of catalyst. The removal of the efficiencies of 10, 20, 30, 40, and 50 ppm were 92.1%, 79.4%, 61.3%, 44.7%, and 33.2%, respectively, and the error bars were found around ±1.8% to ±2.5%. The degradation efficiencies decreased by increasing the concentration of AY42. The decrease in removal effectiveness of degradation is caused by a lack of active sites with a small amount of catalyst, and a lack of light penetration depth combined with the catalyst at the bottom of the reactor for the pollutant's photodegradation activities under visible light.

3.6. Effect of Catalyst Amount. Figure 9 shows the analysis of different catalyst amounts for the photocatalytic degradation removal of AY42 with high concentrations. In this experiment, 50 ppm of AY42 was selected with different catalyst amounts of 20, 40, 60, 80, and 100 mg with a degradation efficiency of 33.2%, 48.1%, 55.3%, 53.1%, and 49.5%, respectively. The result shows that the degradation efficiency increased by increasing the catalyst amount because of the active surface sites. However, the excess amount of catalyst reduced the degradation efficiency of AY42 due to the increase of the catalyst amount, which may decrease the light penetration and thus decrease the light scattering due to the blurry solution.

3.7. Mechanism of Degradation of AY42. In the mechanism process of the degradation of AY42, $K_2Cr_2O_7$, IPA, KI, and 3% La/Bi_2S_3 were used to scavenge the electron, hydroxyl radical, and hole, respectively, in the trapping test (Figure 10(a)). This study looked into the species that are responsible for degrading AY42. The result denoted that the La/Bi_2S_3 electron was coupled with oxygen to create superoxide, which reacted with AY42 to degrade it. Additionally, the role of the Lanthanum ion (La^{3+}) was utilized to improve the photogenerated electron of Bi_2S_3 and to determine the quick recombination of electron-hole pairs

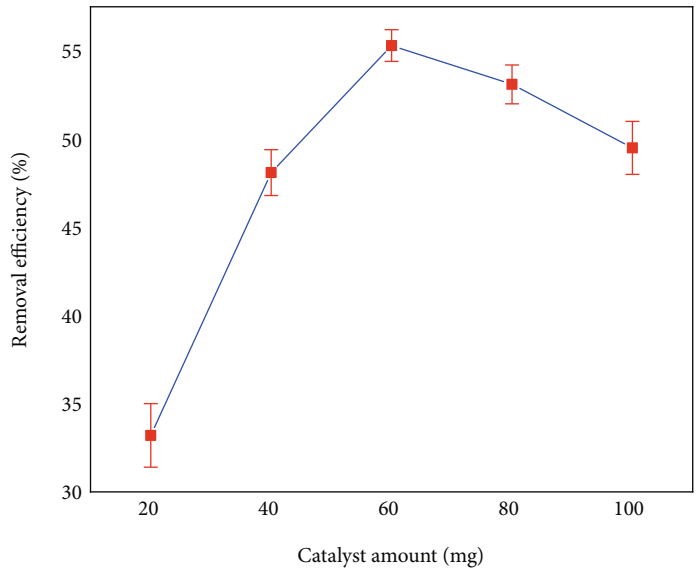

Figure 9: Effect of catalyst amount.

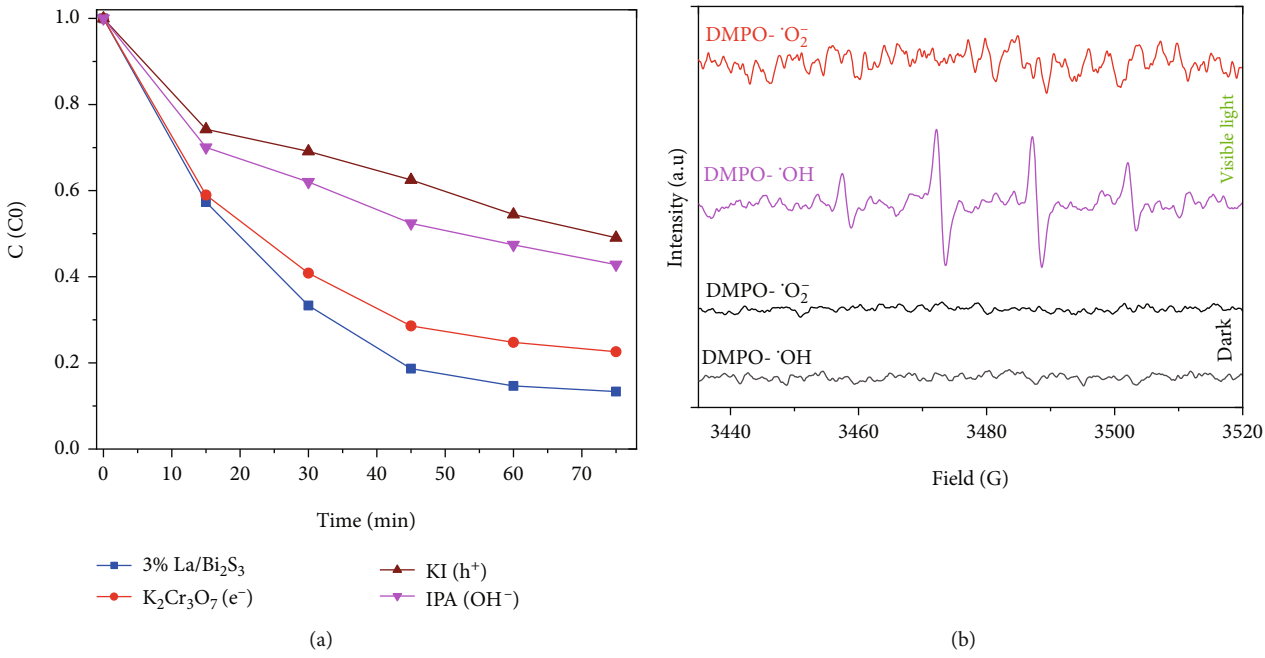

Figure 10: Trapping test (a), electron spin resonance spectra (b).

for improved photodegradation of AY42. The trapping test shows that the degradation efficiency of the AY42 scavenger by $K_2Cr_2O_7$ was decreased from 92.1% to 77.41%, explaining that the electrons were not the most crucial key in the degradation process. In this scavenger, the degradation efficiency decreased from 92.1% to 57.16% in the scavenger by IPA. The material's noticeable drop in photocatalytic activity after adding IPA is due to both radical •OH radicals created directly and radical •OH radicals formed via intermediary processes that were repressed [34], which is the principal active species in the photodegradation activity. The hole (h^+) shows its importance in the degradation of AY42 and explains that OH^- was the intermediate oxidative species.

Furthermore, the ESR spectra of 3% La/Bi_2S_3 (Figure 10(b)) during 12 min under visible light also confirmed that the hydroxyl radicals were the main factor for the degradation of AY42. The DMPO-ESR analysis also demonstrated the detection of the signal when the light was turned on. However, there is almost no signal projected in the dark. This mechanism confirms that the photodegradation of AY42 by the superoxide ($\bullet O_2$) and hydroxide ($^{\bullet}OH$) under visible light was successfully applied.

The photodegradation mechanism of AY42 present in Figure 11 is as follows: Under visible light irradiation, the excited electrons move from the valence band (VB) to the conduction band (CB), and the holes (h^+) stay in VB, as

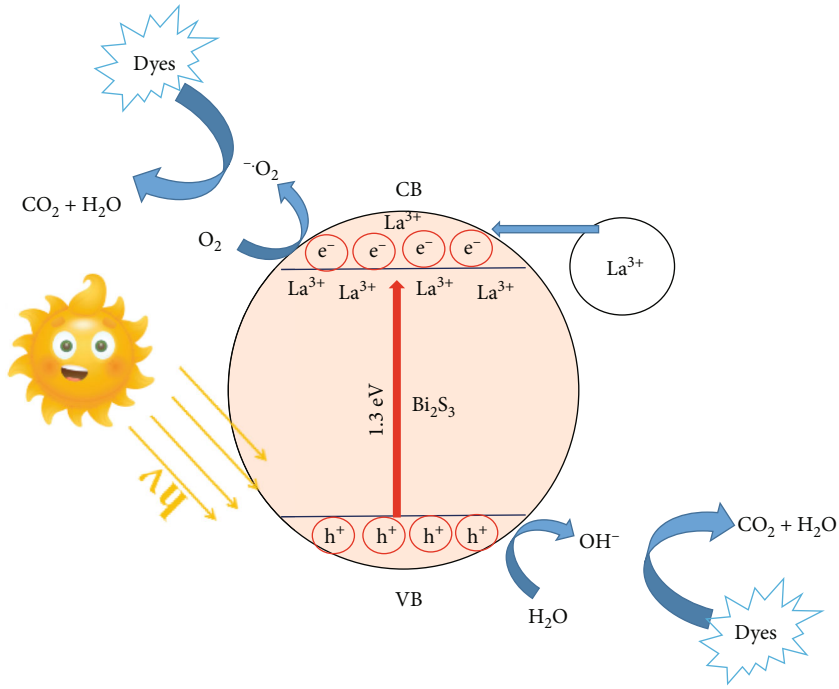

Figure 11: Degradation mechanism of AY42 under visible light.

shown in Equation (2). Then, the electrons (e^-) reacted with oxygen to produce $^{\bullet}O_2^-$ (Equation (3)). La was used to support the CB to avoid the recombination of the photogenerated e^- and h^+ of the catalyst. Adding La species to Bi_2S_3 can significantly increase the formation of $^{\bullet}O_2^-$ radicals and the efficient separation of photogenerated electron-hole pairs, resulting in improved photocatalytic AY42 elimination [35]. The H_2O continually reacted with O_2^- to produce $^{\bullet}OH$ radicals in Equations (4)–((6)()). h^+ combines with OH^- from Equations (4) and (6) for the formation of OH; the holes subsequently reacted with water (Equation (7))). The radicals (O_2^- and OH) were keys to the degradation of AY42, as shown in Equations (8) and (9) [36].

$$La/Bi_2S_3 + hv \longrightarrow La/Bi_2S_3\left(e_{CB}^- + h_{VB}^+\right), \quad (2)$$

$$O_2 + e^- \longrightarrow {}^{\bullet}O_2^-, \quad (3)$$

$$H_2O + {}^{\bullet}O_2^- \longrightarrow OH^- + {}^{\bullet}HO_2, \quad (4)$$

$$H_2O + {}^{\bullet}HO_2 \longrightarrow {}^{\bullet}OH + H_2O_2, \quad (5)$$

$$e^- + H_2O_2 \longrightarrow OH^- + {}^{\bullet}OH, \quad (6)$$

$$H_2O + h^+ \longrightarrow H^+ + {}^{\bullet}OH, \quad (7)$$

$$AY42 + {}^{\bullet}OH \longrightarrow CO_2 + H_2O, \quad (8)$$

$${}^{\bullet}O_2 + AY42 \longrightarrow CO_2 + H_2O. \quad (9)$$

4. Conclusion

This present study proved the hydrothermal method's successful synthesis of La/Bi2S3 material and confirmed by the EDS analysis. The XRD and the particle size analysis showed that the presence of La decreased the crystallites of the Bi_2S_3 material and the La/Bi_2S_3 is indicated as high photodegradation of AY42 dye under visible light. The optimum photocatalytic activities were detected at 3% La/Bi_2S_3, two times more than the pure Bi_2S_3. The trapping test and ESR spectra analysis proved that the hydroxyl radical was the most efficient active species in this photocatalytic process and the h^+ showed its importance in the degradation of AY42 by detecting that OH^- as the intermediate species for the degradation of AY42. The 3% La/Bi_2S_3 could be considered a stable catalyst due to the low percentage of its removal efficiency after reusing this composite four times for the photocatalytic degradation of AY42. Finally, the whole experiment concluded that La greatly influenced a vital role in Bi_2S_3 by modifying the material's structure for the optimization of degradation of AY42 under visible light.

Data Availability

In our manuscript, we provided supporting information as a word document, applied for Section 2.1.

Conflicts of Interest

The authors in this study declare no competing financial interests.

Acknowledgments

We want to present our gratitude to Chung Yuan Christian University. The financial source of this research was Chung Yuan Christian University (Project No: 109609432), which sponsors all the material characterization fees.

Supplementary Materials

Table S1. Presentation of C.I. Acid Yellow 42. *(Supplementary Materials)*

References

[1] H. Grabi, F. Derridj, W. Lemlikchi, and E. Guénin, "Studies of the potential of a native natural biosorbent for the elimination of an anionic textile dye Cibacron Blue in aqueous solution," *Scientific Reports*, vol. 11, no. 1, p. 9705, 2021.

[2] M. Dissanayake, N. Liyanage, C. Herath, S. Rathnayake, and E. Y. Fernando, "Mineralization of persistent azo dye pollutants by a microaerophilic tropical lake sediment mixed bacterial consortium," *Environmental Advances*, vol. 3, article 100038, 2021.

[3] S. Popa, M. E. Radulescu-Grad, A. Perdivara, and G. Mosoarca, "Aspects regarding colour fastness and adsorption studies of a new azo- stilbene dye for acrylic resins," *Scientific Reports*, vol. 11, no. 1, p. 5889, 2021.

[4] N. Y. Donkadokula, A. K. Kola, and D. Saroj, "Modelling and optimization studies on decolorization of brilliant green dye using integrated nanofiltration and photocatalysis," *Sustainable Environment Research*, vol. 30, no. 1, 2020.

[5] http://www.worlddyevariety.com/acid-dyes/acid-yellow-42.html.

[6] C. Espinoza, J. Romero, L. Villegas, L. Cornejo, and R. Salazar, "Mineralization of the textile dye Acid Yellow 42 by solar photoelectro-Fenton in a lab-pilot plant," *Journal of Hazardous Materials*, vol. 319, pp. 24–33, 2016.

[7] R. M. Santos, R. G. Gonçalves, V. R. Constantino et al., "Adsorption of Acid Yellow 42 dye on calcined layered double hydroxide: effect of time, concentration, pH and temperature," *Applied Clay Science*, vol. 140, pp. 132–139, 2017.

[8] Y. Kulshrestha and Q. Husain, "Decolorization and degradation of acid dyes mediated by salt fractionated turnip (Brassica rapa) peroxidases," *Toxicological and Environmental Chemistry*, vol. 89, no. 2, pp. 255–267, 2007.

[9] D. F. Fatimah, T. Harmawantika, I. Sahroni, A. Kamari, C. Sa'bana Rahmatillah, and R. Nurillahi, "Functionalization of hydroxyapatite derived from cockle (Anadara granosa) shells into hydroxyapatite–nano TiO_2 for photocatalytic degradation of methyl violet," *Environmental Research*, vol. 29, no. 1, p. 40, 2019.

[10] E. Fenelon, S.-J. You, and Y.-F. Wang, "Photodegradation of nitrogen oxide under solar light using a facile synthesis catalyst," *Aerosol and Air Quality Research*, vol. 21, no. 10, article 210128, 2021.

[11] A. J. Bard, "Photoelectrochemistry," *Science*, vol. 207, no. 4427, pp. 139–144, 1980.

[12] S. Phanichphant, A. Nakaruk, K. Chansaenpak, and D. Channei, "Evaluating the photocatalytic efficiency of the $BiVO_4$/rGO photocatalyst," *Scientific Reports*, vol. 9, no. 1, p. 16091, 2019.

[13] I. Ali, G.-B. Han, and J.-O. Kim, "Reusability and photocatalytic activity of bismuth-TiO_2 nanocomposites for industrial wastewater treatment," *Environmental Research*, vol. 170, pp. 222–229, 2019.

[14] S. Wang, H. Yang, Z. Yi, and X. Wang, "Enhanced photocatalytic performance by hybridization of Bi_2WO_6 nanoparticles with honeycomb-like porous carbon skeleton," *Journal of Environmental Management*, vol. 248, article 109341, 2019.

[15] Y. Wu, S. Zhou, T. He, X. Jin, and L. Lun, "Photocatalytic activities of $ZnWO_4$ and Bi@$ZnWO_4$ nanorods," *Applied Surface Science*, vol. 484, pp. 409–413, 2019.

[16] H. Bao, C. M. Li, X. Cui, Y. Gan, Q. Song, and J. Guo, "Synthesis of a highly ordered single-crystalline Bi_2S_3 nanowire array and its metal/semiconductor/metal back-to-back Schottky diode," *Small*, vol. 4, no. 8, pp. 1125–1129, 2008.

[17] D.-B. Li, L. Hu, Y. Xie et al., "Low-temperature-processed amorphous Bi_2S_3 film as an inorganic electron transport layer for perovskite solar cells," *ACS Photonics*, vol. 3, no. 11, pp. 2122–2128, 2016.

[18] B. Sun, J. Dong, W.-J. Shi, and S.-Y. Ai, "A hierarchical charge transport cascade based on W-Bi_2S_3/poly (thiophenyl-3-boronic acid) hybrid for robust photoelectrochemical analysis of subgroup J of avian leukosis virus," *Sens Actuators B Chem*, vol. 229, pp. 75–81, 2016.

[19] G. Nie, X. Lu, J. Lei, L. Yang, and C. Wang, "Facile and controlled synthesis of bismuth sulfide nanorods-reduced graphene oxide composites with enhanced supercapacitor performance," *Electrochimica Acta*, vol. 154, pp. 24–30, 2015.

[20] D. Guo, C. Hu, and C. Zhang, "First-principles study on doping and temperature dependence of thermoelectric property of Bi_2S_3 thermoelectric material," *Materials Research Bulletin*, vol. 48, no. 5, pp. 1984–1988, 2013.

[21] Z. G-q, Y.-j. Zheng, Z.-g. He, Z.-x. Lu, L. Wang, and L. C-f, "Synthesis of Bi_2S_3 microsphere and its efficient photocatalytic activity under visible-light irradiation," *Transactions of Nonferrous Metals Society of China*, vol. 28, no. 10, pp. 2002–2010, 2018.

[22] T. Wu, X. Zhou, H. Zhang, and X. Zhong, "Bi_2S_3 nanostructures: a new photocatalyst," *Nano Research*, vol. 3, no. 5, pp. 379–386, 2010.

[23] Y. Huang, J.-J. Cao, F. Kang, S.-J. You, C.-W. Chang, and Y.-F. Wang, "High selectivity of visible-light-driven La-doped TiO_2 photocatalysts for NO removal," *Aerosol and Air Quality Research*, vol. 17, no. 10, pp. 2555–2565, 2017.

[24] E. Fenelon, A. Hussain, T.-H. Yang et al., "High photocatalyst module on degradation of extracted gas from soil under visible light," *Aerosol and Air Quality Research*, vol. 9, no. 12, pp. 2865–2878, 2019.

[25] P. Li, X. Chen, L. Ma, A. Bhat, Y. Li, and J. W. Schwank, "Effect of Ce and La dopants in Co_3O_4 nanorods on the catalytic activity of CO and C_3H_6 oxidation," *Catalysis Science & Technology*, vol. 9, no. 5, pp. 1165–1177, 2019.

[26] W. Raza, M. M. Haque, M. Muneer, M. Fleisch, A. Hakki, and D. Bahnemann, "Photocatalytic degradation of different chromophoric dyes in aqueous phase using La and Mo doped TiO_2 hybrid carbon spheres," *Journal of Alloys and Compounds*, vol. 632, pp. 837–844, 2015.

[27] X. Rong, F. Qiu, J. Rong et al., "Synthesis of porous g-C_3N_4/La and enhanced photocatalytic activity for the degradation of phenol under visible light irradiation," *Journal of Solid State Chemistry*, vol. 230, pp. 126–134, 2015.

[28] E. Fenelon, D.-P. Bui, H. H. Tran et al., "Straightforward synthesis of SnO_2/Bi_2S_3/BiOCl–$Bi_{24}O_{31}Cl_{10}$ composites for drastically enhancing rhodamine B photocatalytic degradation under visible light," *ACS Omega*, vol. 5, no. 32, pp. 20438–20449, 2020.

[29] D. Onwudiwe and V. Nkwe, "Morphological variations in Bi_2S_3 nanoparticles synthesized by using a single source precursor," *Heliyon*, vol. 6, no. 7, article e04505, 2020.

[30] M. Liu, L. Wang, P. Dong et al., "Correlation between types of defects/vacancies of Bi_2S_3 nanostructures and their transient photocurrent," *Nano Research*, vol. 10, no. 7, pp. 2405–2414, 2017.

[31] J. Cao, B. Xu, H. Lin, B. Luo, and S. Chen, "Novel heterostructured Bi_2S_3/BiOI photocatalyst: facile preparation, characterization and visible light photocatalytic performance," *Dalton Transactions*, vol. 41, no. 37, pp. 11482–11490, 2012.

[32] S. Jiang, K. Zhou, Y. Shi et al., "In situ synthesis of hierarchical flower-like Bi_2S_3/BiOCl composite with enhanced visible light photocatalytic activity," *Applied Surface Science*, vol. 290, pp. 313–319, 2014.

[33] S. Boughdachi, Y. Badali, Y. Azizian-Kalandaragh, and S. Altindal, "Current-transport mechanisms of the Al/(Bi_2S_3-PVA nanocomposite)/p-Si Schottky diodes in the temperature range between 220 K and 380 K," *Journal of Electronic Materials*, vol. 47, no. 12, pp. 6945–6953, 2018.

[34] T. H. Huy, D. P. Bui, F. Kang et al., "SnO_2/TiO_2 nanotube heterojunction: the first investigation of NO degradation by visible light-driven photocatalysis," *Chemosphere*, vol. 215, pp. 323–332, 2019.

[35] M.-T. Pham, T.-M. T. Nguyen, D.-P. Bui, Y.-F. Wang, H.-H. Tran, and S.-J. You, "Enhancing quantum efficiency at Ag/g-C_3N_4 interfaces for rapid removal of nitric oxide under visible light," *Sustainable Chemistry and Pharmacy*, vol. 25, no. 100596, p. 100596, 2022.

[36] S. Y. Lee, D. Kang, S. Jeong, H. T. Do, and J. H. Kim, "Photocatalytic degradation of rhodamine B dye by TiO_2 and gold nanoparticles supported on a floating porous polydimethylsiloxane sponge under ultraviolet and visible light irradiation," *ACS Omega*, vol. 5, no. 8, pp. 4233–4241, 2020.

[37] Z. Zhang, W. Wang, L. Wang, and S. Sun, "Enhancement of visible-light photocatalysis by coupling with narrow-band-gap semiconductor: a case study on Bi_2S_3/Bi_2WO_6," *ACS Applied Materials & Interfaces*, vol. 4, no. 2, pp. 593–597, 2012.

[38] H. Demir, Ö. Şahin, O. Baytar, and S. Horoz, "Investigation of the properties of photocatalytically active Cu-doped Bi_2S_3 nanocomposite catalysts," *Journal of Materials Science: Materials in Electronics*, vol. 31, no. 13, pp. 10347–11054, 2020.

[39] M. Lu, G. Yuan, Z. Wang, Y. Wang, and J. Guo, "Synthesis of $BiPO_4$/Bi_2S_3 heterojunction with enhanced photocatalytic activity under visible-light irradiation," *Nanoscale Research Letters*, vol. 10, no. 1, p. 385, 2015.

[40] Y. Huang, W. Fan, B. Long et al., "Visible light Bi_2S_3/Bi_2O_3/$Bi_2O_2CO_3$ photocatalyst for effective degradation of organic pollutions," *Applied Catalysis B: Environmental*, vol. 185, pp. 68–76, 2016.

[41] W. Xu, J. Fang, Y. Chen et al., "Novel heterostructured Bi_2S_3/$Bi_2Sn_2O_7$ with highly visible light photocatalytic activity for the removal of rhodamine B," *Materials Chemistry and Physics*, vol. 154, pp. 30–37, 2015.